Electronic Supplementary Material (ESI) for Chemical Science.

Supporting information for the manuscript

Geometrical Influence on Non-Biomimetic Heterolytic Splitting of H_2 by Bio-Inspired [FeFe]-Hydrogenase Complexes: a rare example of *inverted* Frustrated Lewis Pair based reactivity.

Lucile Chatelain,*[a] Jean-Baptiste Breton,[a] Federica Arrigoni,*[b] Philippe Schollhammer*[a] and Giuseppe Zampella*[b]

[a] UMR CNRS 6521 Chimie, Electrochimie Moléculaires et Chimie Analytique, Université de Bretagne Occidentale, UFR Sciences et Techniques, 6 Avenue Victor le Gorgeu, CS 93837, Brest-Cedex 3, 29238 France

[b] Department of Biotechnology and Bioscience, University of Milano-Bicocca, Piazza della Scienza 2, 20126 Milan, Italy

Contents

I. NMR spectra

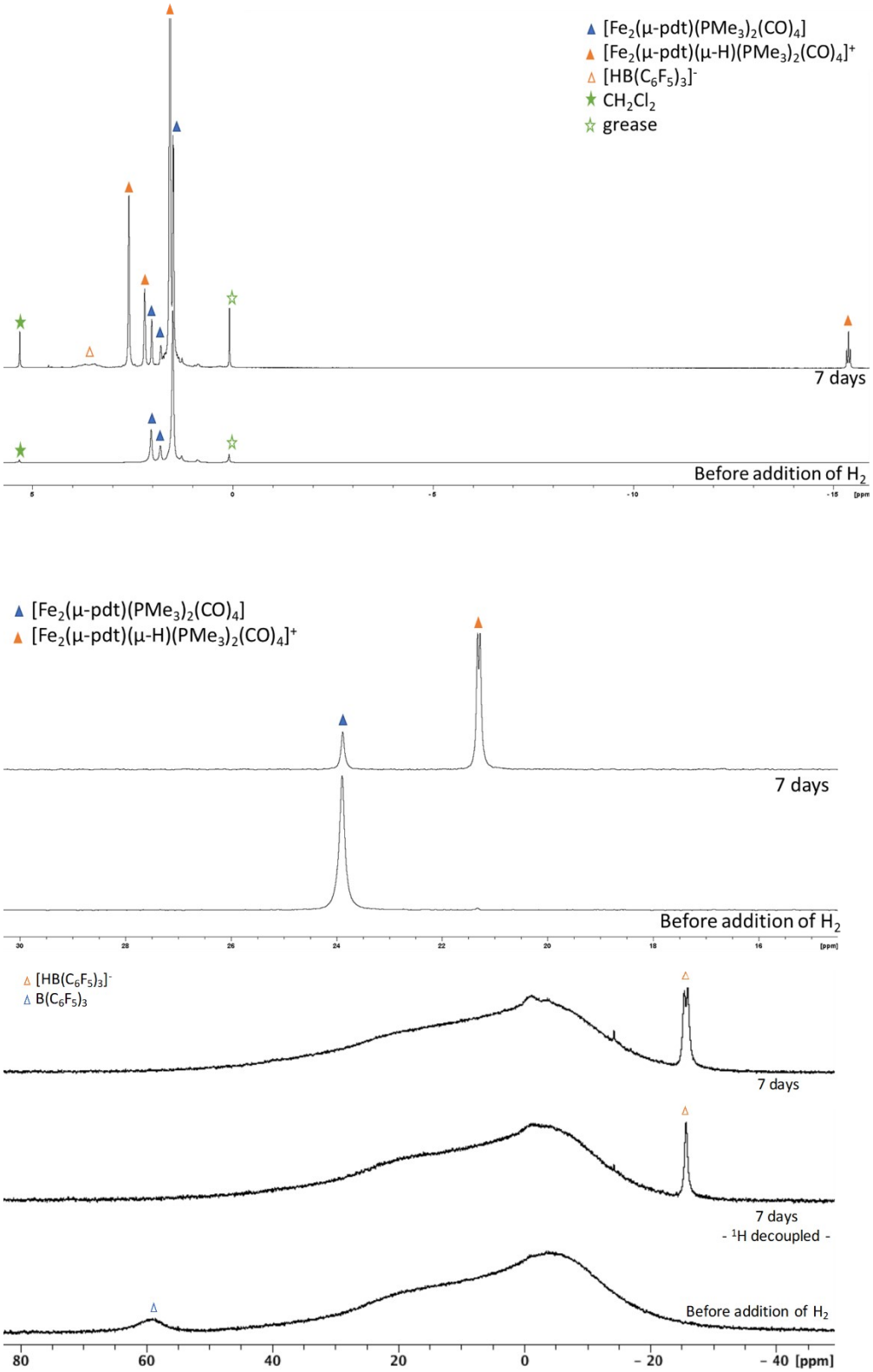

Figure S1: ^{1}H (400 MHz) (top), ^{31}P (161.97 MHz) (middle) and ^{11}B (128.38 MHz) (bottom) NMR spectra of a 1:1 solution of $[Fe_2(\mu\text{-pdt})(PMe_3)_2(CO)_4]$: $B(C_6F_5)_3$ in CD_2Cl_2 exposed 7 days to H_2

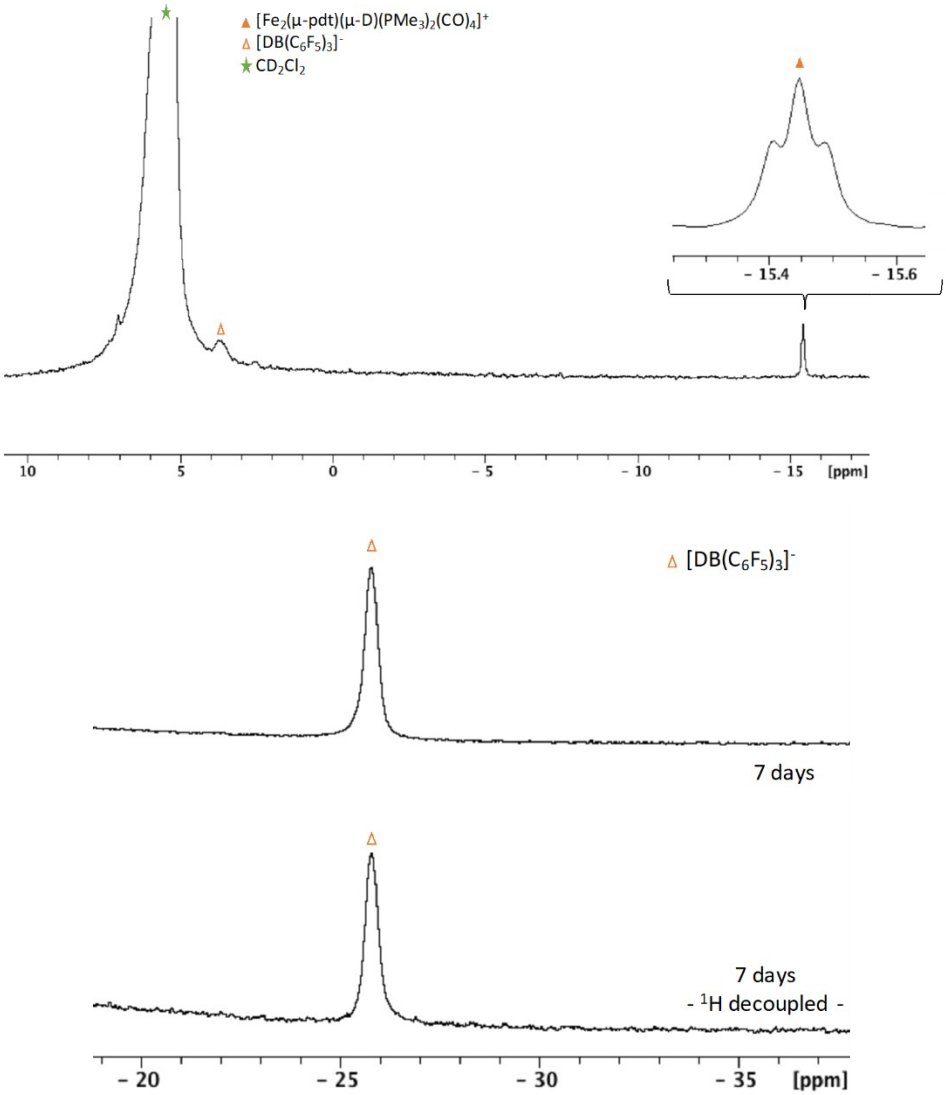

Figure S2: ^{2}H (76.77 MHz) (top) and ^{11}B (160.46 MHz) (bottom) NMR spectra of a 1:1 solution of $[Fe_2(\mu\text{-pdt})(PMe_3)_2(CO)_4]$: $B(C_6F_5)_3$ in CD_2Cl_2 exposed 7 days to D_2

NMR of the isolated product $[Fe_2(\mu\text{-pdt})(\mu\text{-H})(PMe_3)_2(CO)_4][HB(C_6F_5)_3]$

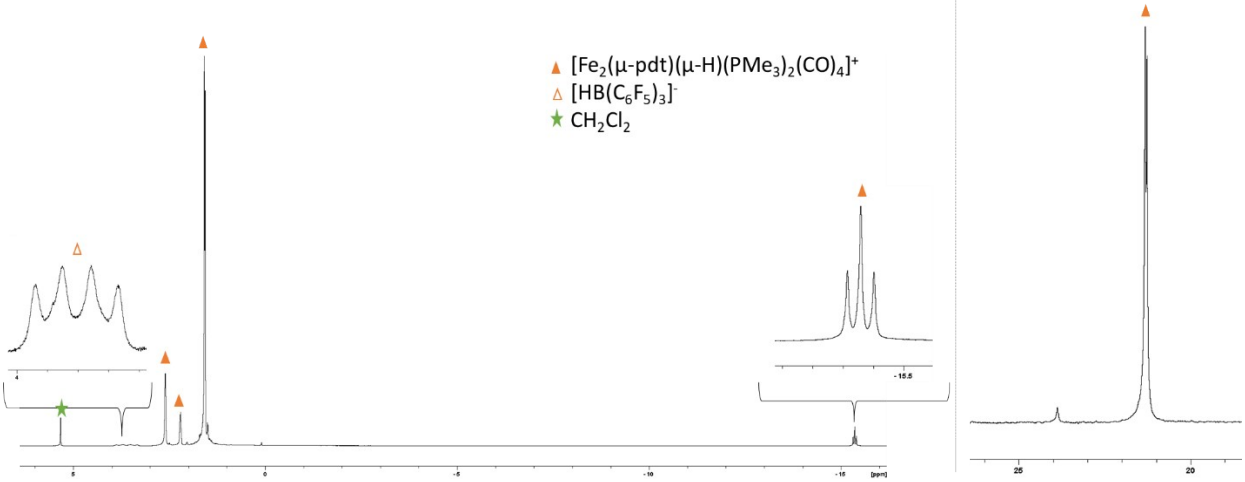

Figure S3: NMR (298K, CD_2Cl_2) spectra of $[Fe_2(\mu\text{-pdt})(\mu\text{-H})(PMe_3)_2(CO)_4][HB(C_6F_5)_3]$ (left) ^{1}H (500 MHz) and (right) ^{31}P (202.46 MHz)

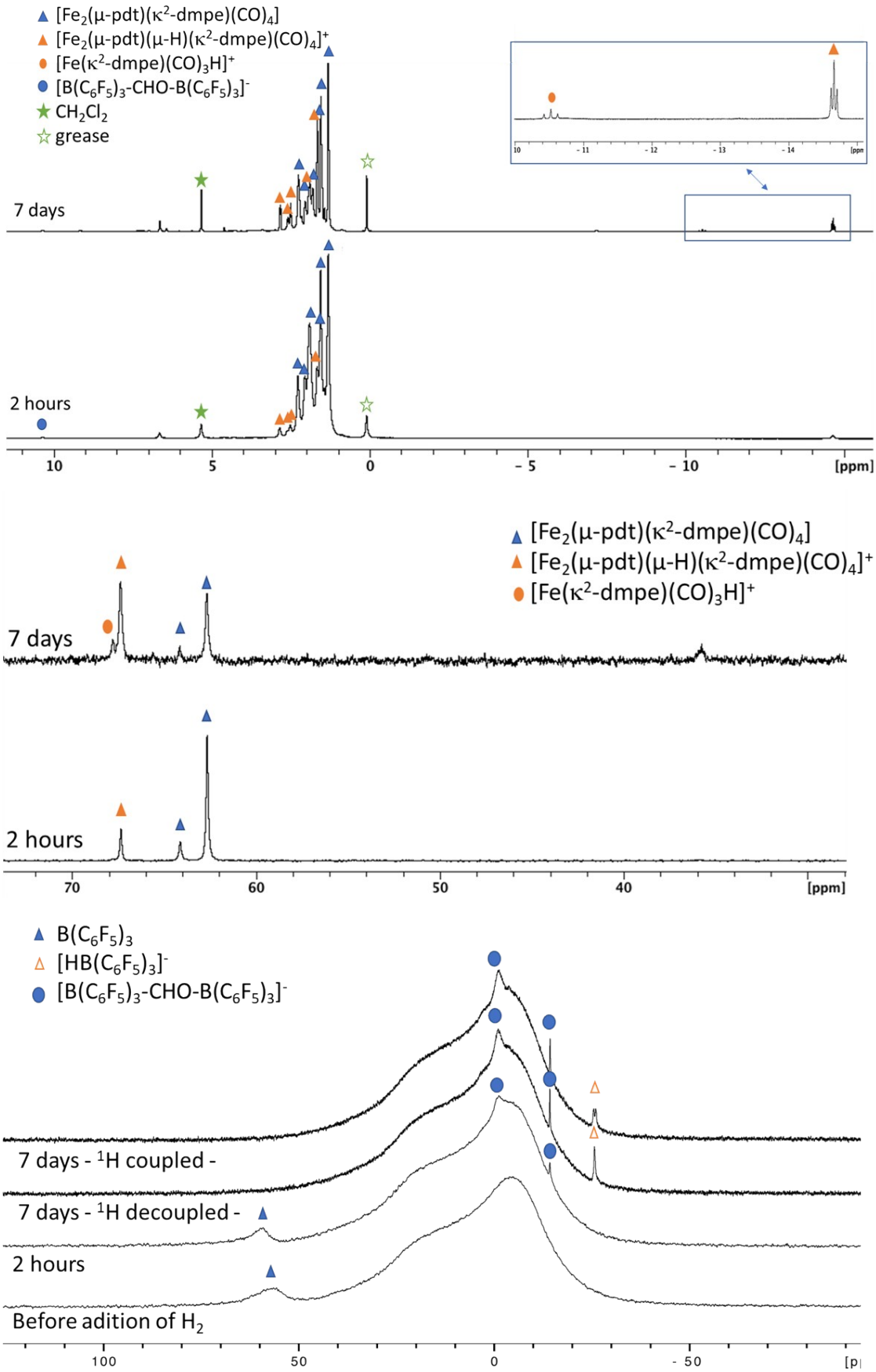

Figure S4: NMR (298K, CD_2Cl_2) spectra of a mixture of $B(C_6F_5)_3$ and $[Fe_2(\mu\text{-pdt})(\kappa^2\text{-dmpe})(CO)_4]$ in presence of H_2 : (top) ^1H (500 MHz), (middle) ^{31}P (202.46 MHz) and (bottom) ^{11}B (160.46 MHz)

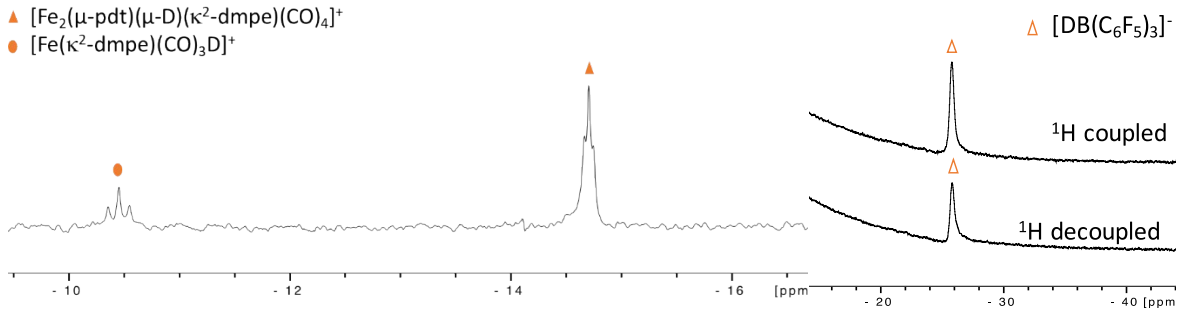

Figure S5: NMR spectra of the solid dissolved in CD_2Cl_2 after the reaction of $B(C_6F_5)_3$ and $[Fe_2(\mu\text{-pdt})(\kappa^2\text{-dmpe})(CO)_4]$ in presence of D_2 in CD_2Cl_2: (left) ^2H (76.77 MHz) and (right) ^{11}B (28.38 MHz)

NMR of the isolated product $[Fe_2(\mu\text{-pdt})(\mu\text{-H})(\kappa^2\text{-dmpe})(CO)_4][HB(C_6F_5)_3]$

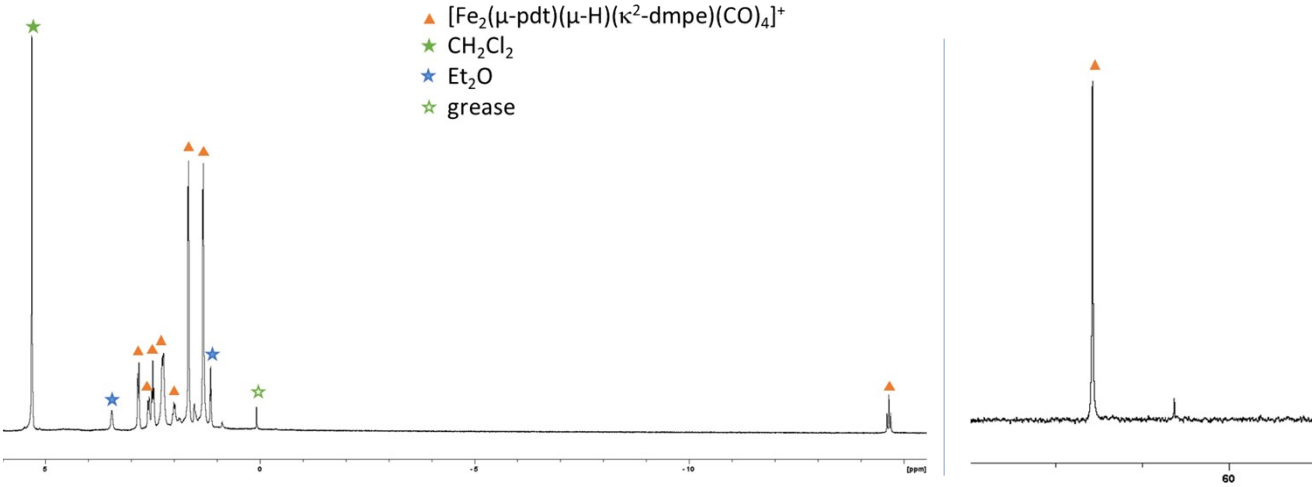

Figure S6: NMR (298K, CD_2Cl_2) spectra of $[Fe_2(\mu\text{-pdt})(\mu\text{-H})(\kappa^2\text{-dmpe})(CO)_4][HB(C_6F_5)_3]$ (left) ^1H (500 MHz) and (right) ^{31}P (202.46 MHz)

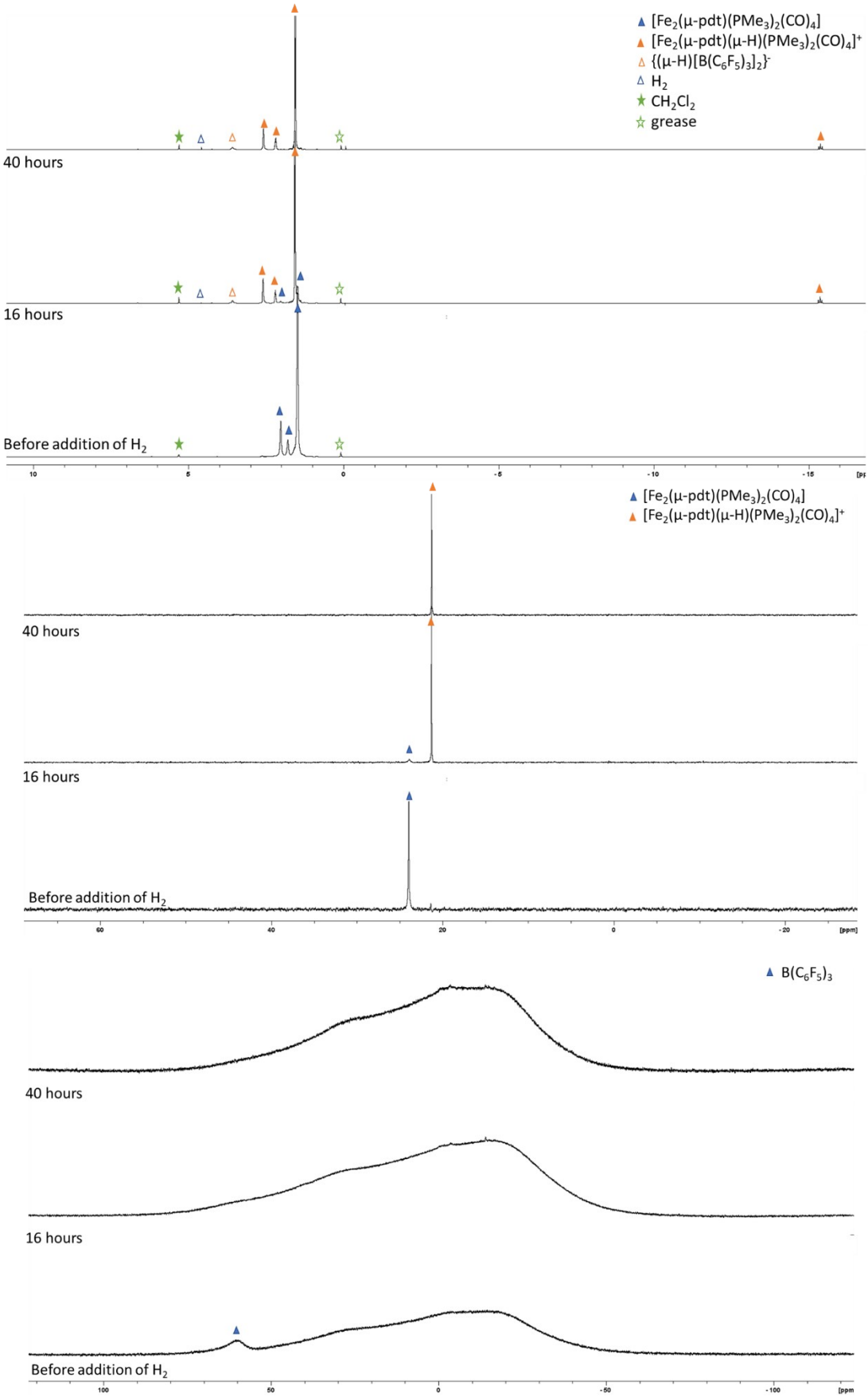

Figure S7: ^{1}H (400 MHz) (top), ^{31}P (161.97 MHz) (middle) and ^{11}B (128.38 MHz) (bottom) NMR spectra of a 1:2 solution of $[Fe_2(\mu\text{-pdt})(PMe_3)_2(CO)_4]$: $B(C_6F_5)_3$ in CD_2Cl_2 exposed 2 days to H_2 at 298 K

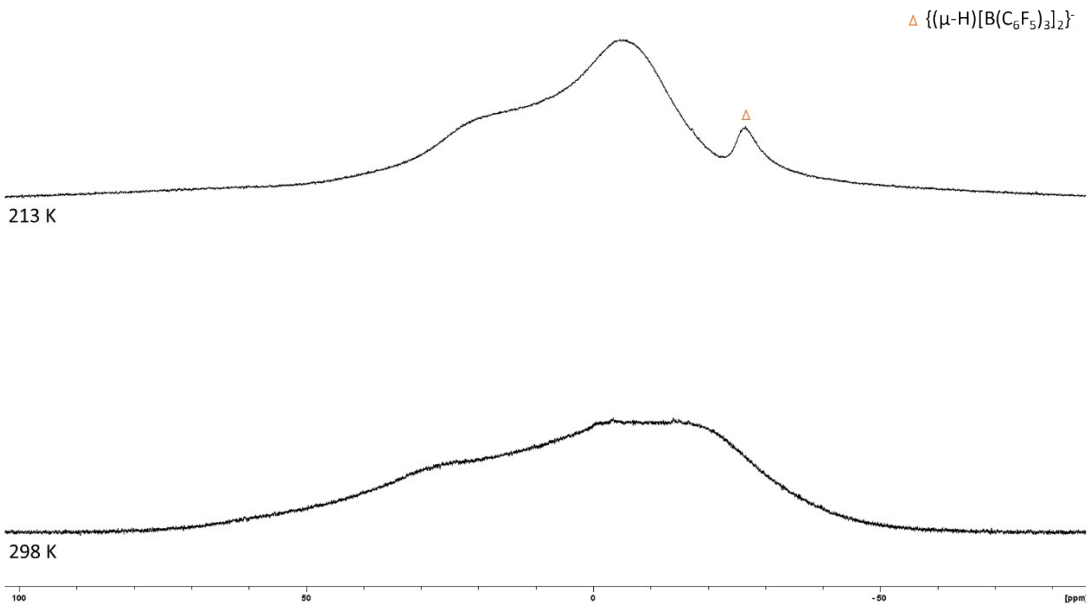

Figure S8: ^{11}B (128.38MHz (bottom) and 160.46 MHz (top)) NMR spectra of a 1:2 solution of $[Fe_2(\mu\text{-}pdt)(PMe_3)_2(CO)_4]$: $B(C_6F_5)_3$ in CD_2Cl_2 after 2 days of H_2 exposure recorded at 298 K and 213 K

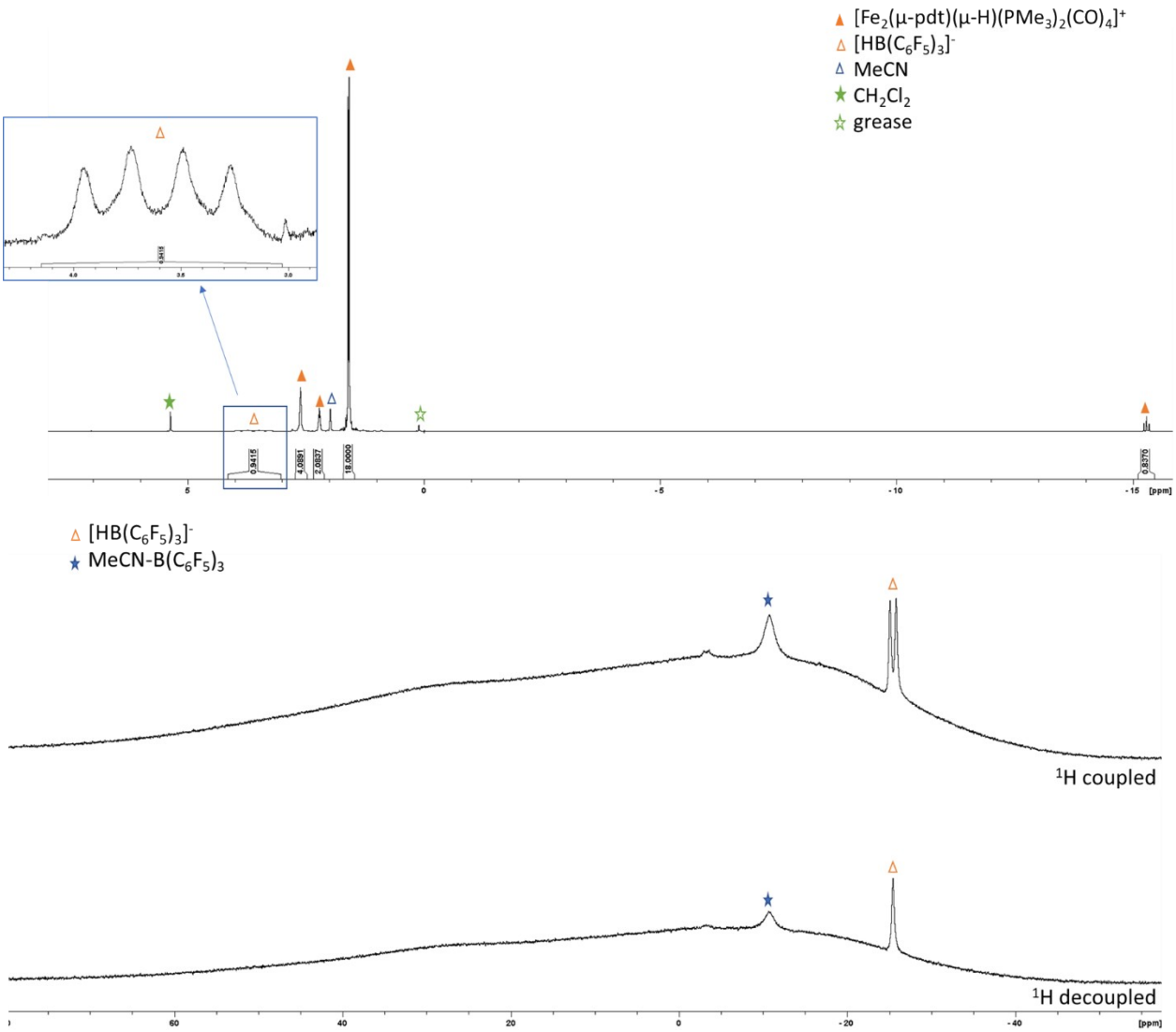

Figure S9: ^{1}H (500 MHz) (top) and ^{11}B (160.46 MHz) (bottom) NMR spectra of a solution of $[Fe_2(\mu\text{-}pdt)(PMe_3)_2(CO)_4][(C_6F_5)_3B\text{-}(\mu\text{-}H)\text{-}B(C_6F_5)_3]$ in CD_2Cl_2 after addition of MeCN at 298 K

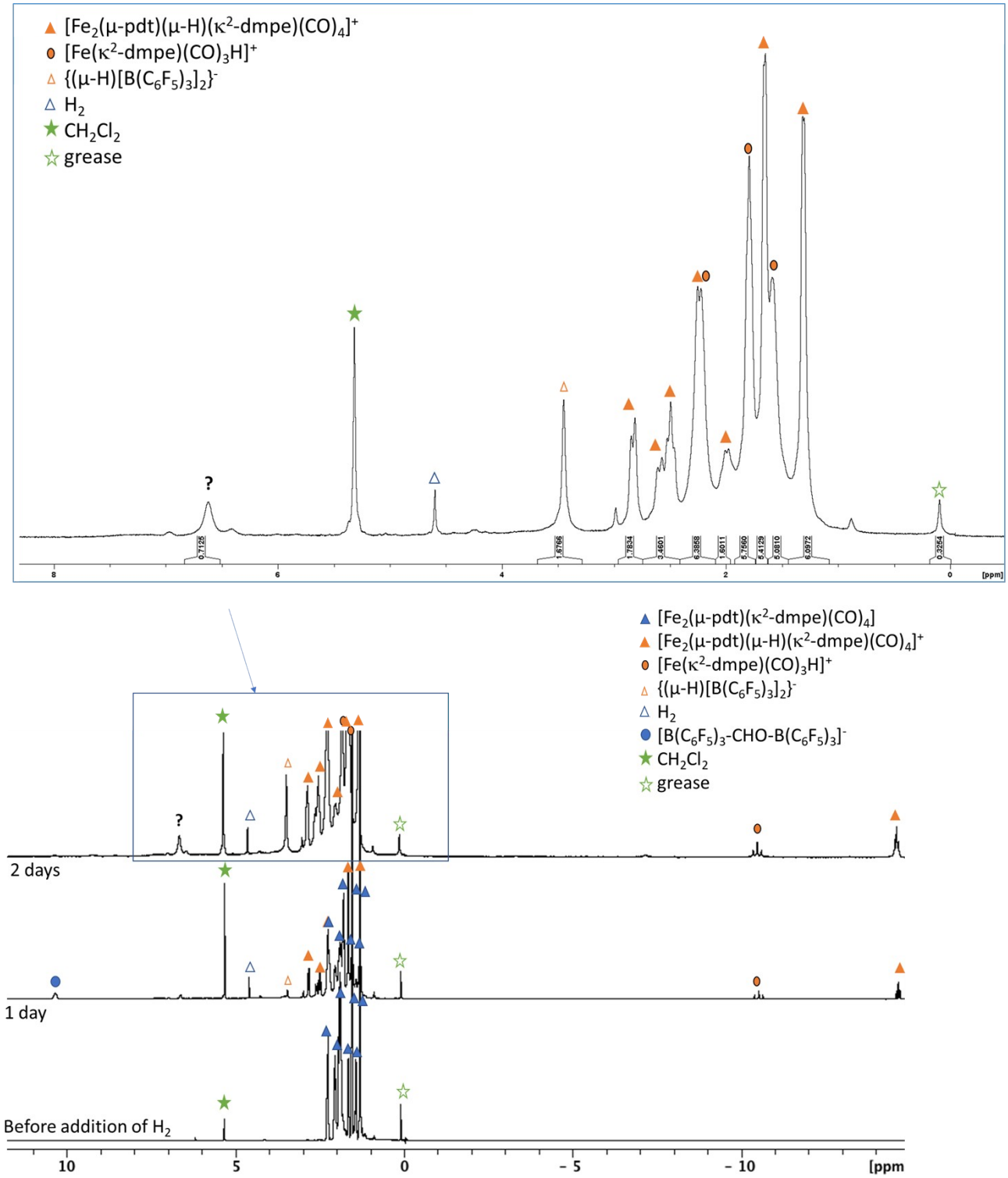

Figure S10: ^{1}H NMR (400 MHz, 298K) spectra of the solution mixture $[Fe_2(\mu\text{-pdt})(\kappa^2\text{-dmpe})(CO)_4]$ and 2 equivalents of $B(C_6F_5)_3$ in CD_2Cl_2 before and after addition of H_2

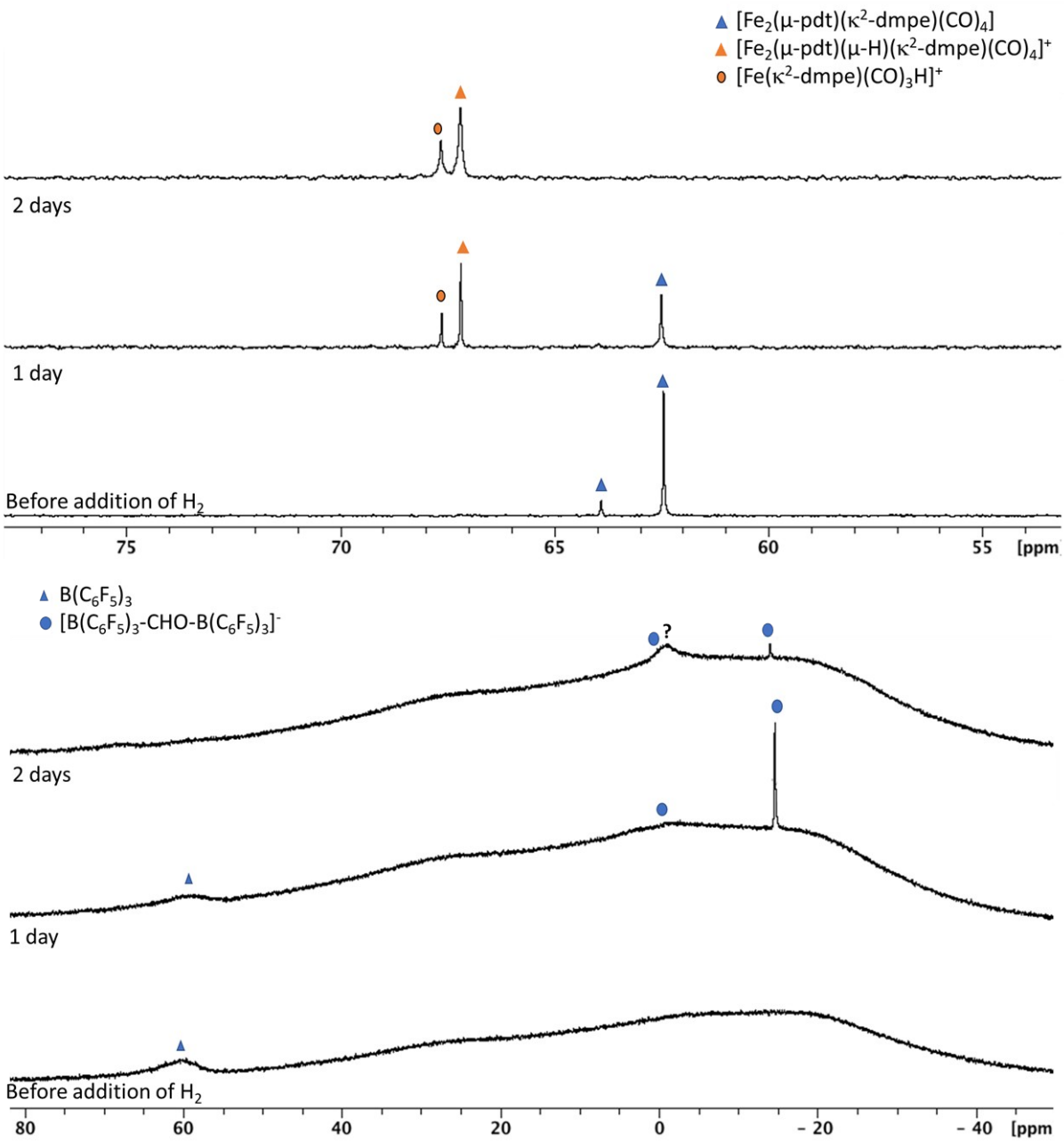

Figure S11: NMR (298K, CD_2Cl_2) spectra of the solution mixture [$Fe_2(\mu$-pdt)(κ^2-dmpe)$(CO)_4$] and 2 equivalents of $B(C_6F_5)_3$ in CD_2Cl_2 before and after addition of H_2 (top) ^{31}P (161.97 MHz) and (bottom) ^{11}B (128.38 MHz)

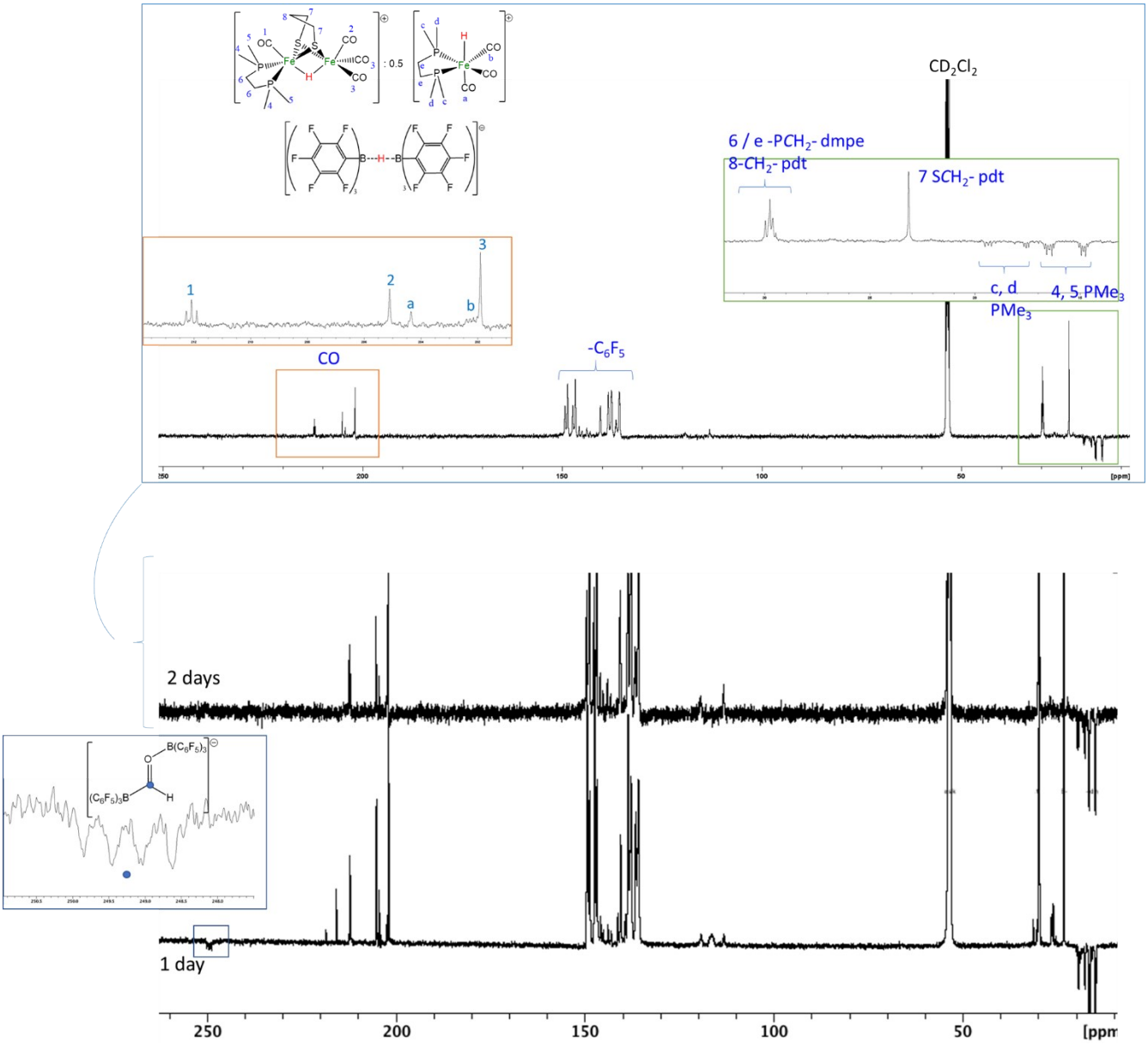

Figure S12: ^{13}C (125.76 MHz, 298 K) NMR spectra of the solution mixture $[Fe_2(\mu\text{-pdt})(\kappa^2\text{-dmpe})(CO)_4]$ and 2 equivalents of $B(C_6F_5)_3$ in CD_2Cl_2 after addition of H_2 showing the disappearance of the formyl borate species after 2 days at room temperature

Low temperature experiments

To a J. Young NMR tube containing both solids of $B(C_6F_5)_3$ (0.043 mmol, 1 equiv.) and **2** (0.043 mmol, 1 equiv.) was added under a 1 atm. pressure of H_2 0.5 mL of cold CD_2Cl_2 (-70°C). The tube was kept at -70°C until its introduction to the precooled NMR spectrometer. NMR analysis were then carried on.

A terminal hydride species $[Fe_2(\mu\text{-pdt})(H_t)(\kappa^2\text{-dmpe})(CO)_4]^+$ is formed and remains observable until 253 K. At higher temperature it converts into the apical-basal and basal-basal bridging hydride isomers $[Fe_2(\mu\text{-pdt})(\mu\text{-H})(\kappa^2\text{-dmpe})(CO)_4]^+$, the thermodynamic complex is the only isomer remaining after one night at room temperature. The second hydride arising from the H_2 splitting forms a broad singlet at room temperature at 6.6 ppm (defined as a triplet at 203 K (J = 16 Hz)) probably due to the stabilization of an unidentified structure between hydride and $B(C_6F_5)_3$. Once formed at low temperature this species is stable at room temperature and addition of MeCN allows the formation of the known hydrido-borate anion $[HB(C_6F_5)_3]^-$.

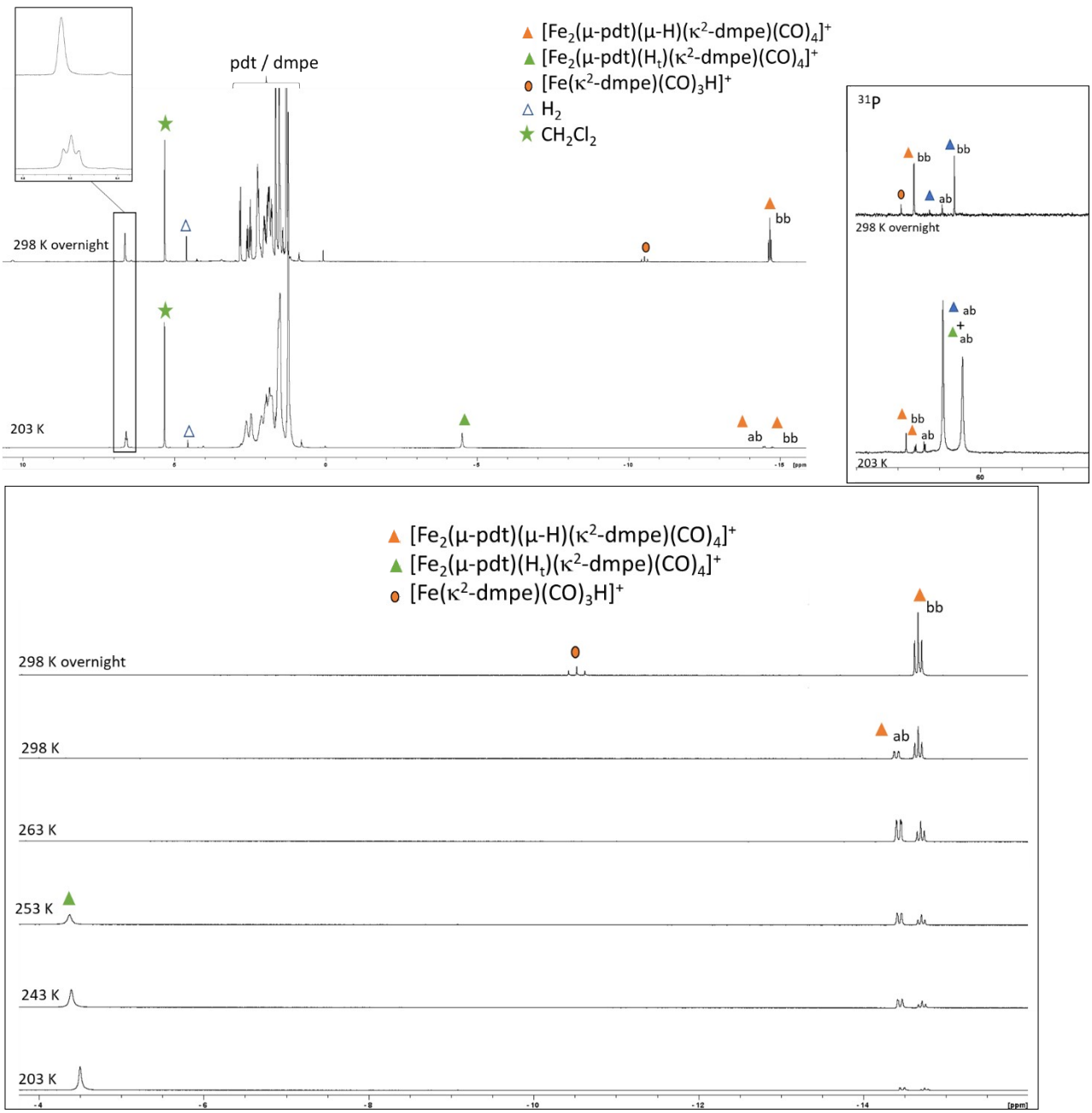

Figure S13. ^{1}H (500 MHz) NMR spectra and inserts of ^{31}P (202.46 MHz) and ^{1}H NMR spectra at the negative region of a 1:1 solution of $[Fe_2(\mu\text{-pdt})(\kappa^2\text{-dmpe})(CO)_4]$: $B(C_6F_5)_3$ in CD_2Cl_2 exposed to H_2 at -70°C and recorded at 203 K before warming up to reach 298K.

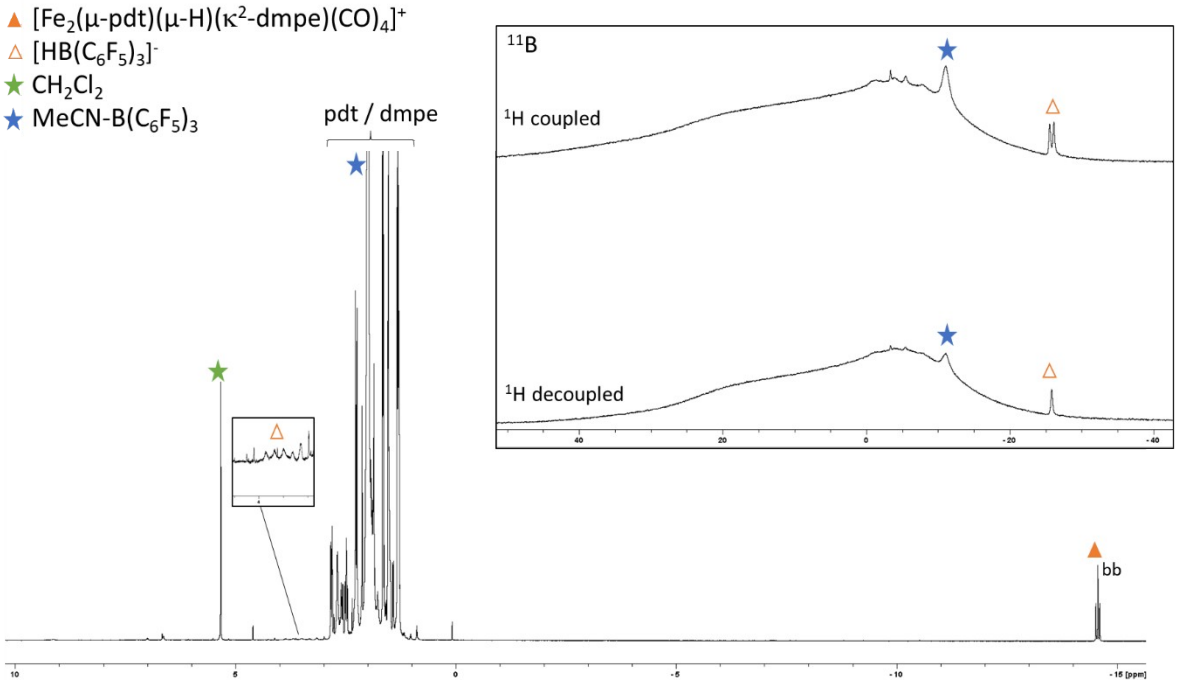

Figure S14. ^{1}H (500 MHz) NMR spectra and inserts of ^{11}B (160.46 MHz) of a 1:1 solution of $[Fe_2(\mu\text{-}pdt)(\kappa^2\text{-}dmpe)(CO)_4]$: $B(C_6F_5)_3$ in CD_2Cl_2 initially exposed to H_2 at -70°C and let stabilized at 298K before addition of MeCN, showing the conversion of the broad singlet at 6.6 ppm in ^{1}H NMR to the known quadruplet of the $[HB(C_6F_5)_3]^-$ anion at 3.5 ppm. The ^{11}B NMR spectra also revealed the formation of this same anion together with the MeCN-$B(C_6F_5)_3$ adduct.

Reactivity using $B(C_6H_5)_3$ instead of $B(C_6F_5)_3$

A CD_2Cl_2 solution of $B(C_6H_5)_3$ (0.052 mmol, 1 equiv.) and **1** or **2** (0.052 mmol, 1 equiv.) in J. Young NMR tube was exposed to H_2 (1 atm.) and followed by NMR analysis for 5 days. No reactivity was observed.

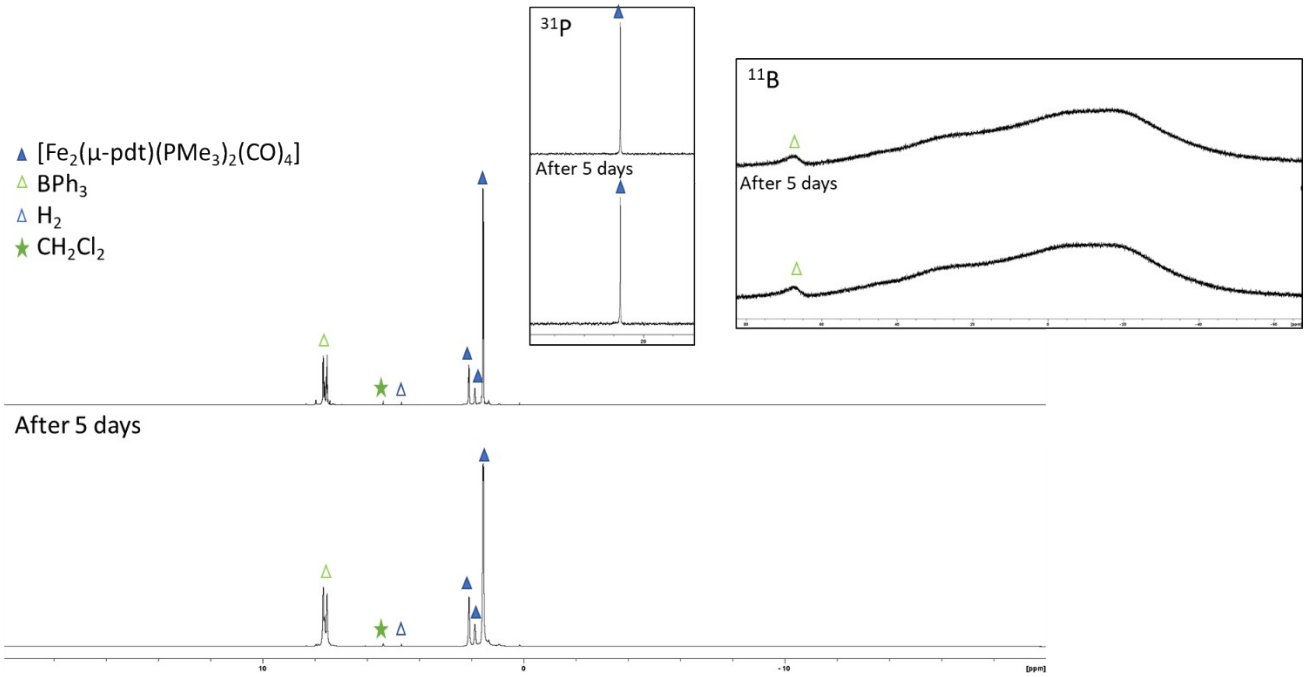

Figure S15. ^{1}H (400 MHz) and inserts of ^{31}P (161.97 MHz) and ^{11}B (128.38 MHz) NMR spectra of a 1:1 solution of $[Fe_2(\mu\text{-}pdt)(PMe_3)_2(CO)_4]$: $B(C_6H_5)_3$ in CD_2Cl_2 after 5 days of H_2 exposure recorded at 298 K

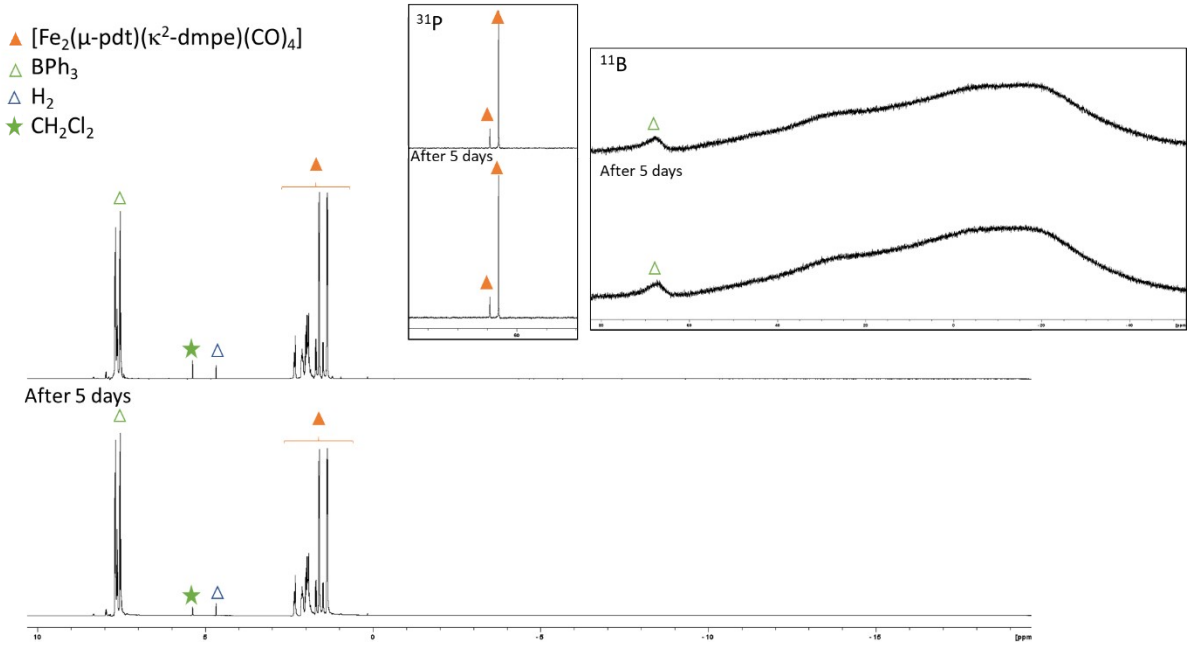

Figure S16. ^{1}H (400 MHz) and inserts of ^{31}P (161.97 MHz) and ^{11}B (128.38 MHz) NMR spectra of a 1:1 solution of $[Fe_2(\mu\text{-pdt})(\kappa^2\text{-dmpe})(CO)_4]$: $B(C_6H_5)_3$ in CD_2Cl_2 after 5 days of H_2 exposure recorded at 298 K

Activation of H_2O

The addition of 5 equiv. of H_2O to a CD_2Cl_2 solution of **1** (0.041 mmol, 1 equiv.) and $B(C_6F_5)_3$ (0.041 mmol, 1 equiv.) in J. Young NMR tube was followed by NMR analysis and revealed the conversion of **1** into the bridging hydride cation $[Fe_2(\mu\text{-pdt})(\mu\text{-H})(PMe_3)_2(CO)_4]^+$ in 50% yield. The ^{11}B NMR did not reveal any distinctive resonance.

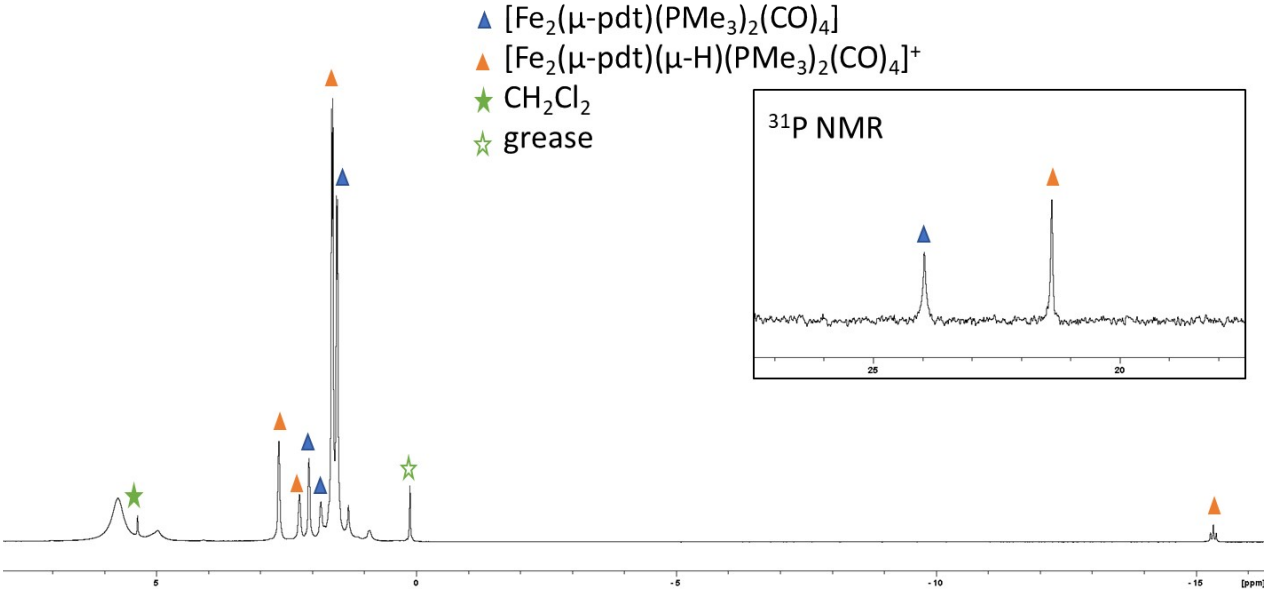

Figure S17: ^{1}H (400MHz, 298K) and insert ^{31}P (161.98 MHz, 298K) NMR spectra of a 1:1 solution of $[Fe_2(\mu\text{-pdt})(PMe_3)_2(CO)_4]$: $B(C_6F_5)_3$ in CD_2Cl_2 in presence of 5equiv. H_2O after 24h

II. IR spectra

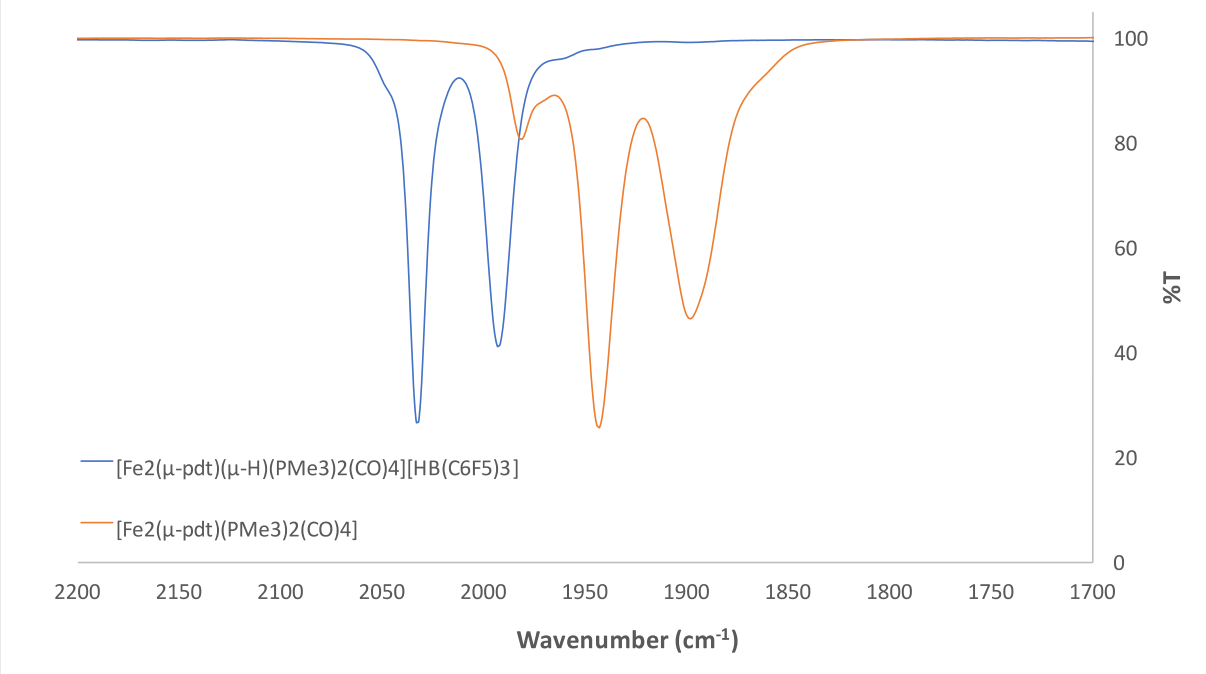

Figure S18: IR spectra of $[Fe_2(\mu\text{-pdt})(\mu\text{-H})(PMe_3)_2(CO)_4][HB(C_6F_5)_3]$ and $[Fe_2(\mu\text{-pdt})(PMe_3)_2(CO)_4]$ in CH_2Cl_2 solution

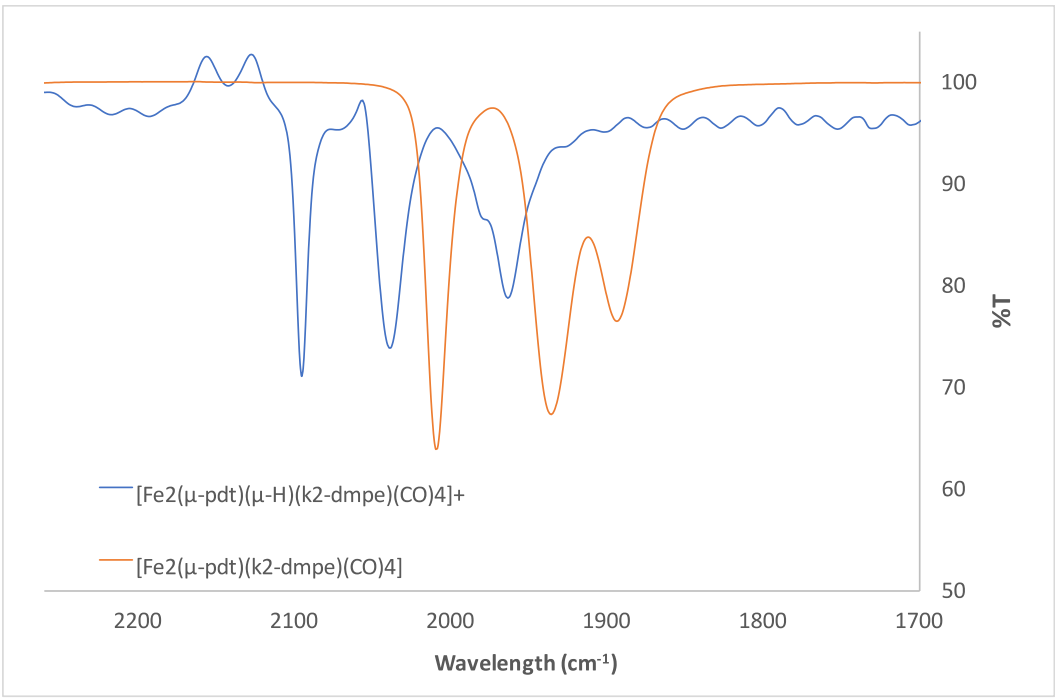

Figure S19: IR spectra of $[Fe_2(\mu\text{-pdt})(\mu\text{-H})(\kappa^2\text{-dmpe})(CO)_4][HB(C_6F_5)_3]$ and $[Fe_2(\mu\text{-pdt})(\kappa^2\text{-dmpe})(CO)_4]$ in CH_2Cl_2 solution

III. DFT calculations

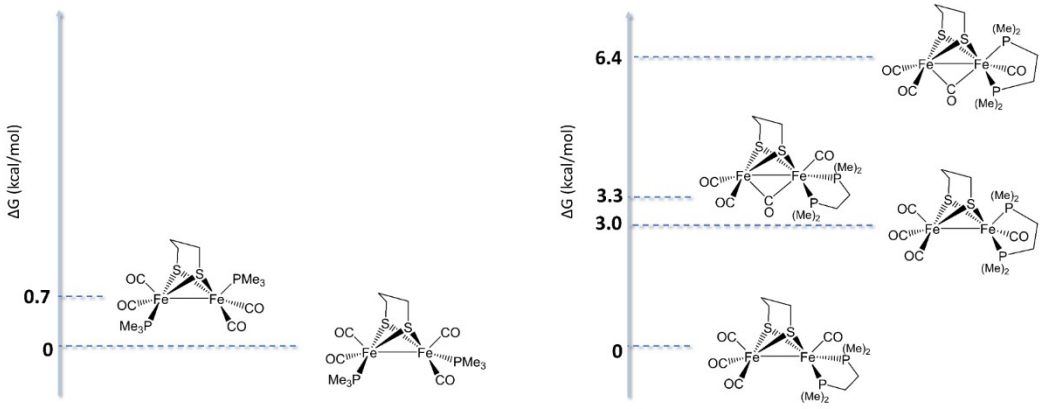

*Figure S20: Relative stability between basal-basal and apical-basal isomers of **1** (left) and **2** (right).*

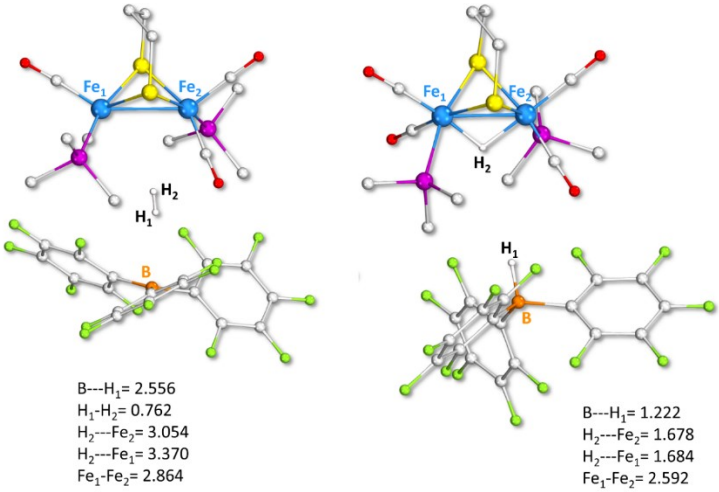

*Figure S21: Optimized structure of selected intermediates. Reactant (left) and product (right) of the H_2 splitting step in **1**, along **1-TS$_{bb}$** (see Figure 1). Selected distances are in Å. Colors legend: grey = carbon; red = oxygen; light blue = iron; purple = phosphorus; yellow = sulfur; orange = boron; green = fluorine.*

BP86-D3 NBO	Fe1	Fe2	H1	H2	B
$\mathbf{1}_{bb}$	-0,15	-0,15	-0,02	0,01	0,75
$\mathbf{1\text{-}TS}_{bb}$	-0,23	-0,19	0,04	-0,04	0,26
$\mathbf{1}_{ab}$	-0,22	-0,20	0,00	0,01	0,79
$\mathbf{1\text{-}TS}_{ab}$	-0,21	-0,19	0,12	-0,08	0,26
$\mathbf{2}_{bb}$	-0,18	-0,15	-0,04	0,01	0,75
$\mathbf{2\text{-}TS}_{bb}$	-0,18	-0,16	-0,05	-0,03	0,2
$\mathbf{2}_{ab}$	-0,15	-0,13	-0,04	0,00	0,74
$\mathbf{2\text{-}TS}_{ab}$	-0,16	-0,14	-0,01	-0,03	0,16
$\mathbf{2\text{-}Int}_{bb}$	-0,33	-0,32	0,12	0,00	0,09
$\mathbf{2\text{-}Int}_{ab}$	-0,34	-0,27	0,11	0,02	0,04
Löwdin	**Fe1**	**Fe2**	**H1**	**H2**	**B**
$\mathbf{1}_{bb}$	-0,62	-0,60	0,03	0,01	0,01
$\mathbf{1\text{-}TS}_{bb}$	-0,64	-0,63	0,11	0,07	-0,21
$\mathbf{1}_{ab}$	-0,63	-0,63	0,04	0,04	0,02
$\mathbf{1\text{-}TS}_{ab}$	-0,63	-0,63	0,14	0,04	-0,13
$\mathbf{2}_{bb}$	-0,69	-0,56	0,03	0,01	0,02
$\mathbf{2\text{-}TS}_{bb}$	-0,68	-0,54	0,08	0,04	-0,26
$\mathbf{2}_{ab}$	-0,65	-0,54	0,04	0,04	0,01
$\mathbf{2\text{-}TS}_{ab}$	-0,66	-0,52	0,11	0,05	-0,24
$\mathbf{2\text{-}Int}_{bb}$	-0,56	-0,73	0,13	0,06	-0,27
$\mathbf{2\text{-}Int}_{ab}$	-0,58	-0,70	0,13	0,05	-0,29

B3LYP-D3 NBO	Fe1	Fe2	H1	H2	B
$\mathbf{1}_{bb}$	-0,12	-0,11	-0,05	0,01	0,82
$\mathbf{1\text{-}TS}_{bb}$	-0,2	-0,13	-0,06	0,02	0,28
$\mathbf{1}_{ab}$	-0,2	-0,17	0,00	0,01	0,85
$\mathbf{1\text{-}TS}_{ab}$	-0,19	-0,15	0,13	-0,11	0,33
$\mathbf{2}_{bb}$	-0,18	-0,07	0,01	0,04	0,82
$\mathbf{2\text{-}TS}_{bb}$	-0,16	-0,06	-0,08	-0,05	0,22
$\mathbf{2}_{ab}$	-0,16	-0,05	-0,05	0,04	0,82
$\mathbf{2\text{-}TS}_{ab}$	-0,13	-0,04	0,06	0,03	0,18
$\mathbf{2\text{-}Int}_{bb}$	-0,25	-0,32	0,12	-0,02	0,12
$\mathbf{2\text{-}Int}_{ab}$	-0,32	-0,21	0,11	0,01	0,07
Löwdin	**Fe1**	**Fe2**	**H1**	**H2**	**B**
$\mathbf{1}_{bb}$	-0,75	-0,75	0,00	0,03	-0,06
$\mathbf{1\text{-}TS}_{bb}$	-0,8	-0,75	0,12	0,07	-0,31
$\mathbf{1}_{ab}$	-0,76	-0,75	0,04	0,04	-0,06
$\mathbf{1\text{-}TS}_{ab}$	-0,76	-0,75	0,14	0,07	-0,21
$\mathbf{2}_{bb}$	-0,8	-0,72	0,01	0,04	-0,05
$\mathbf{2\text{-}TS}_{bb}$	-0,79	-0,69	0,11	0,03	-0,31
$\mathbf{2}_{ab}$	-0,63	-0,57	0,02	0,03	0,04
$\mathbf{2\text{-}TS}_{ab}$	-0,75	-0,73	0,12	0,07	-0,35
$\mathbf{2\text{-}Int}_{bb}$	-0,59	-0,72	0,13	0,05	-0,26
$\mathbf{2\text{-}Int}_{ab}$	-0,59	-0,69	0,12	0,04	-0,28

Table S1: NBO and Löwdin analysis for selected species, performed at the BP86-D3 and B3LYP-D3 (single point calculations on BP86-D3 optimized geometries) levels. For atom numbering refer to Figure 1, 2 and 3 of the main text.

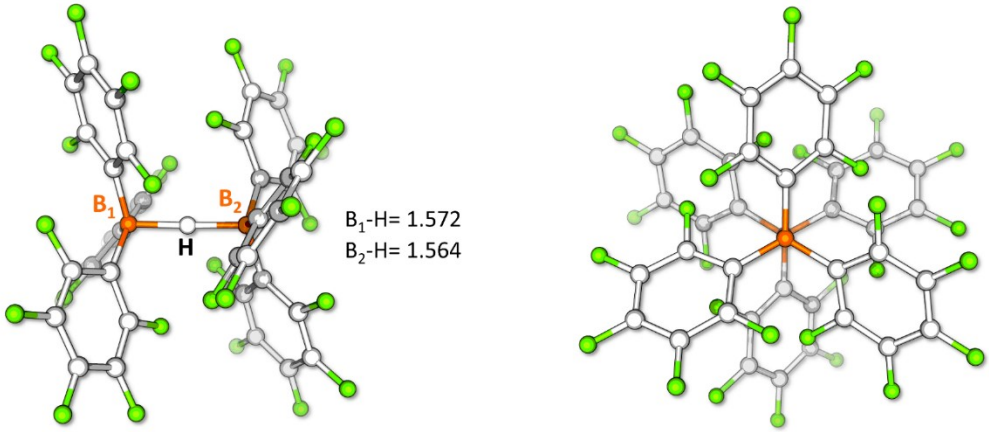

Figure S22: Optimized structures of the $[(C_6F_5)_3B\text{-}(\mu\text{-}H)\text{-}B(C_6F_5)_3]^-$ bridging hydride. This species is formed upon the coupling: $B(C_6F_5)_3 + [HB(C_6F_5)_3]^- \rightarrow [(C_6F_5)_3B\text{-}(\mu\text{-}H)\text{-}B(C_6F_5)_3]^-$, an exergonic process by -10.2 kcal/mol. The ΔG of the coupling has been calculated as free energy difference between the bridging hydride product and a van der Waals adduct formed by one molecule of each reactant. Selected distances are in Å. Colors legend: grey = carbon; red = oxygen; light blue = iron; purple = phosphorus; yellow = sulfur; orange = boron; green = fluorine.